Research article

JHEP|Reports

Cholangiocarcinoma-on-a-chip: A human 3D platform for personalised medicine

Michela Anna Polidoro,[1] Erika Ferrari,[2] Cristiana Soldani,[1] Barbara Franceschini,[1] Giuseppe Saladino,[2] Arianna Rosina,[2] Andrea Mainardi,[2,3] Francesca D'Autilia,[4] Nicola Pugliese,[5,6] Guido Costa,[7] Matteo Donadon,[8,9] Guido Torzilli,[5,7] Simona Marzorati,[1] Marco Rasponi,[2,†] Ana Lleo[5,6,*,†]

[1]*Hepatobiliary Immunopathology Laboratory, IRCCS Humanitas Research Hospital, Rozzano, Milan, Italy;* [2]*Department of Electronics, Information and Bioengineering, Politecnico di Milano, Milan, Italy;* [3]*Department of Biomedicine, University Hospital Basel, University of Basel, Basel, Switzerland;* [4]*Unit of Advanced Optical Microscopy, IRCCS Humanitas Research Hospital, Rozzano, Milan, Italy;* [5]*Department of Biomedical Science, Humanitas University, Pieve Emanuele, Milan, Italy;* [6]*Division of Internal Medicine and Hepatology, Department of Gastroenterology, IRCCS Humanitas Research Hospital, Rozzano, Milan, Italy;* [7]*Division of Hepatobiliary and General Surgery, Department of Surgery, IRCCS Humanitas Research Hospital, Rozzano, Milan, Italy;* [8]*Department of Health Sciences, Università del Piemonte Orientale, Novara, Italy;* [9]*Department of General Surgery, University Maggiore Hospital, Novara, Italy*

JHEP Reports **2024.** https://doi.org/10.1016/j.jhepr.2023.100910

Background & Aims: Cholangiocarcinoma (CCA) is a primary liver tumour characterised by a poor prognosis and limited therapeutic options. Available 3D human CCA models fail to faithfully recapitulate the tumour niche. We aimed to develop an innovative patient-specific CCA-on-chip platform.

Methods: A CCA tumour microenvironment was recapitulated on a microfluidic three-channel chip using primary CCA cells, cancer-associated fibroblasts (CAFs), endothelial cells, and T cells isolated from CCA specimens (n = 6). CAF and CCA cells were co-cultured in the central channel, flanked by endothelial cells in one lateral channel, recreating a tubular structure. An extensive characterisation of this platform was carried out to investigate its diffusion ability, hydrogel properties, and changes in matrix composition. Cell phenotype and functional properties were assessed.

Results: Primary cells seeded on the microfluidic device were shown to reproduce the architectural structure and maintain the original phenotype and functional properties. The tumour niche underwent a deep remodelling in the 3D device, with an increase in hydrogel stiffness and extracellular matrix deposition, mimicking *in vivo* CCA characteristics. T cells were incorporated into the device to assess its reliability for immune cell interaction studies. Higher T cell migration was observed using cells from patients with highly infiltrated tumours. Finally, the drug trial showed the ability of the device to recapitulate different drug responses based on patient characteristics.

Conclusions: We presented a 3D CCA platform that integrates the major non-immune components of the tumour microenvironment and the T cell infiltrate, reflecting the CCA niche. This CCA-on-chip represents a reliable patient-specific 3D platform that will be of help to further elucidate the biological mechanisms involved in CCA and provide an efficient tool for personalised drug testing.

Impact and implications: An innovative patient-specific cholangiocarcinoma (CCA)-on-chip platform was successfully developed, integrating the major components of the tumour microenvironment (tumour cells, cancer-associated fibroblasts, endothelial cells, and immune infiltrate) and faithfully mimicking the CCA niche. This CCA-on-chip represents a powerful tool for unravelling disease-associated cellular mechanisms in CCA and provides an efficient tool for personalised drug testing.

Introduction

Cholangiocarcinoma (CCA) is the second most common primary liver tumour, arising from the malignant transformation of cholangiocytes that line the biliary tree.[1] CCA diagnosis usually occurs at advanced stages owing to the absence of noticeable symptoms.[2] Furthermore, the lack of successful CCA treatments correlates to poor prognosis.[3] Currently, surgical resection represents the only potentially curative treatment. However, only 10–30% of patients present resectable tumours at the time of diagnosis, with a median survival lower than 1 year for unresectable patients.[2,4] This highlights the importance of establishing reliable human CCA models to investigate the pathophysiological mechanisms underlying its progression, along with the development of new efficient therapeutic strategies.[5] These models should be able to faithfully recapitulate the desmoplastic CCA

Keywords: Liver-on-chip; Cholangiocarcinoma; Microfluidics; Tumour microenvironment; Cell–cell crosstalk; Drug testing.
Received 12 June 2023; received in revised form 15 August 2023; accepted 31 August 2023; available online 15 September 2023

† These authors jointly supervised this work.

* Corresponding author. Address: Department of Biomedical Sciences, Humanitas University; Division of Internal Medicine and Hepatology, Department of Gastroenterology, Humanitas Research Hospital IRCCS, Via A. Manzoni 56, Rozzano, Milan, Italy.
E-mail address: ana.lleo@humanitas.it (A. Lleo).

tumour microenvironment (TME), whereby intense crosstalk is established between cancer-associated fibroblasts (CAFs) and tumour cells, leading to the release of several signalling molecules and extracellular matrix (ECM) proteins, fostering CCA proliferation, invasiveness, and drug resistance.[6,7]

In recent years, the organs-on-chip (OoC) model has strongly emerged as a powerful disease model for patient-specific studies, allowing to overcome the limitations of the existing *in vitro* and *in vivo* tumour models through the combination of microfluidics, microfabrication techniques, and tissue engineering.[8] Indeed, OoCs can replicate an *in vivo*-like microenvironment, mimicking cell–cell and cell–ECM interactions, and providing spatiotemporally controlled stimuli. Contrariwise, the routinely used 2D models are not able to recapitulate the TME complexity, whereas in the available 3D *in vitro* models (*e.g.* spheroids, organoids), although cells show an improved architecture and functionality, they grow in a non-dynamic environment.[9,10] Additionally, OoCs can include patient-derived cells, thus allowing the development of patient-specific platforms.[11,12]

Intensive research supports OoCs suitability to investigate human biological mechanisms and to constitute a reliable tool for drug-screening applications. Over time, several healthy and pathological liver-on-chip (LoC) models have been developed, showing to reliably emulate an *in vivo*-like liver architecture with improved cell metabolic functions.[13,14] To the best of our knowledge, CCA-on-chip models have not been developed yet. We herein propose an innovative and functional CCA-on-chip model that faithfully recapitulates the complexity of the CCA microenvironment and provides a reliable platform for personalised drug-screening and mechanistic study of CCA pathogenesis.

Materials and methods

Device design and fabrication

The microfluidic chip, created with AutoCAD (Autodesk, Inc.), comprised three adjacent channels separated by two rows of trapezoidal posts. The central channel was intended for a gel-embedded co-culture of CCA cells and CAFs, while the lateral channels supplied the medium for the cells. After design optimisation, the first mould was obtained by photolithography, performed in PoliFab facilities (Polytechnic of Milan, Milan, Italy) in a class 1,000 cleanroom. A negative photoresist (SU-8, MicroChem corporation) was spin-coated on a silicon wafer and exposed to a collimated UV laser beam, to transfer the desired pattern via the maskless technique. Subsequently, polydimethylsiloxane (PDMS) chips were produced by soft lithography. A curing agent and a base pre-polymer (Sylgard® 184, Dow Corning) were mixed in a 1:10 ratio, poured on the mould and cured for 2 h at 65 °C. Biopsy punchers (Harris Uni-Core, Sigma-Aldrich) were used to create 1-mm diameter access ports at the gel channel inlet and outlet and 8-mm diameter holes at the extremes of the lateral channels, as medium reservoirs. Thereafter, chips were bonded either on a glass coverslip or a PDMS membrane through oxygen plasma treatment (Harrick Plasma Cleaners). The microfluidic devices were autoclaved at 120 °C for 30 min.

Chip seeding protocol

Central channel: hydrogel, and co-culture parameters

Fibrin gel (Tisseel, Baxter) was tested at 5 mg/ml, 10 mg/ml, and 25 mg/ml with thrombin (Tisseel, Baxter) at 2.5 U/ml. Briefly, fibrinogen 100 mg/ml and thrombin 500 U/ml were diluted at the desired working concentration, according to the manufacturer's protocol. Primary cell isolation and cell culture methods are described in the supplementary material and Fig. S1. Tumour cells were mixed with the solution at 4×10^7 cells/ml, injected in the chip central channel and allowed to polymerise at 37 °C for 5 min. Rat tail collagen type I (Corning) hydrogel was tested at 2.5 mg/ml and 5 mg/ml. According to the manufacturer's protocol, collagen hydrogel was prepared by neutralising a 9.1 mg/ml collagen stock solution with 0.22% NaOH, 10% PBS 10× and 5% 4-(2-hydroxyethyl)-1-piperazineethanesulfonic acid (HEPES). Tumour cells were resuspended in the collagen solution and incubated at 37 °C for 20 min to promote gel polymerisation. Moreover, a mixed collagen–fibrin hydrogel (2.5–10 mg/ml) was tested on-chip. Briefly, fibrin and collagen pre-polymeric solutions were prepared according to the desired final concentration, mixed in a 1:1 ratio before injection in the channel and allowed to polymerise at 37 °C for 5 min. A Live/Dead Cell Double Staining Kit (Sigma-Aldrich) was used to analyse cell viability in the central channel, according to the manufacturer's instructions. Gene expression analysis was assessed using Real-time PCR; all primer pair sequences can be found in Table S1.

Lateral channel: endothelial cell seeding protocol

To recreate a tubular structure with the endothelial cells (ECs) in the right lateral channel, after hydrogel polymerisation, the channel was coated with 10 μg/ml fibronectin from human plasma (Sigma-Aldrich) and incubated for 20 min at 37 °C. Then, ECs were injected at 5×10^6 cells/ml into the channel and incubated for 20 min at 37 °C. Subsequently, the chip was rotated 180° and a second ECs inject was performed. This procedure was repeated twice, to promote ECs adhesion to the top and bottom surface of the channel. The device was maintained at 37 °C with 95% humidity and 5% CO_2. The medium was refreshed once daily with the addition of aminocaproic acid (ACA) to prevent hydrogel fibrinolysis (Sigma-Aldrich). The ACA concentrations were as follows: 2 mg/ml on Day 0 and Day 1, 1.6 mg/ml on Day 2, 1.4 mg/ml on Day 3, and 1.2 mg/ml on Day 4.

The schematic protocol of the chip seeding is summarised in Fig. S2.

Drug treatment

Gemcitabine (GEM, solution 100 mg/ml) was purchased from Accord Healthcare. Cisplatin (CDDP, solution 1 mg/ml) was provided by Teva Italia. Drug sensitivity experiments were performed with CCA primary cells (n=5) cultured in the 2D monolayer and in the 3D microfluidic platform, with and without CAFs. Subsequently, based on time to relapse, patients were divided into early (<12 months; n = 2) and late (>12 months; n = 3) recurrence. For the 2D system, CCA primary cells were seeded in 96-well plates (1×10^3 cells/well) and, after 3 days, the cells were incubated with a combination of GEM and CDDP in a ratio 1:5 at different concentrations (0 μM; 50–10 μM; 10–2 μM) for 48 h. Similarly, CCA primary cells were cultured with or without CAFs within the chip for 3 days and subsequently exposed to GEM–CDDP for 48 h. Neither the control medium nor the medium containing GEM/CDDP was supplemented with ACA. The viability of the cells in the 2D system was evaluated using RealTime-Glo® MT cell viability assay (Promega), according to the manufacturer's protocol. Instead, to evaluate cell viability on-chip, CCA cells and CAFs were stained with the

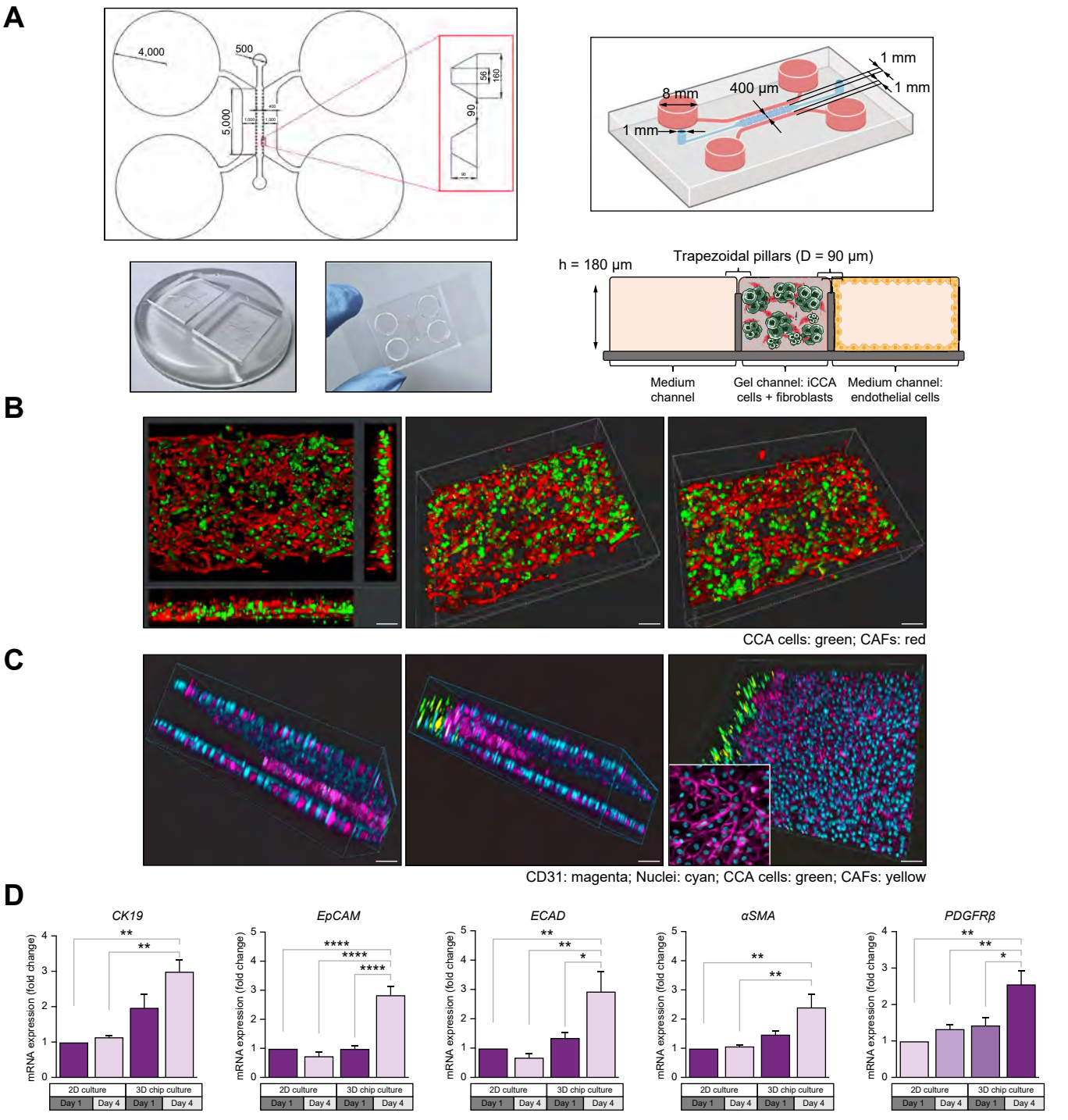

Fig. 1. CCA-on-CHIP. (A) AutoCAD chip design with pillar detail. At the bottom, the resin used for chip serial production with the schematic representation of the CCA-on-CHIP. (B) 3D reconstruction of the chip central channel. Left, the orthogonal view of CCA cells (green) and CAFs (red). Right, volume rendering of z-stack using IMARIS https://imaris.oxinst.com. Scale bar = 80 µm. (C) 3D reconstructions of the endothelial channel. Volume rendering of z-stack using IMARIS. Scale bar = 80 µm. CD31: magenta; nuclei: cyan; CCA cells: green; CAFs: red. (D) Gene expression analysis of CCA cells and CAFs in 2D monolayer and 3D platform. One-way ANOVA (mean ± SEM; n = 5 biological replicates). *p <0.05; **p <0.01; ****p <0.0001. CAFs, cancer-associated fibroblasts; CCA, cholangiocarcinoma.

CellTracker™ Green and Red (Invitrogen). Cell survival was assessed by calculating the percentage of cell viability compared with the control medium (0 µM) at the 48-h time point.

T cells migration assay on-chip

CCA cells and CAFs were stained with CellTracker™ Red (Invitrogen), seeded and cultured on-chip for 4 days. Stimulated or

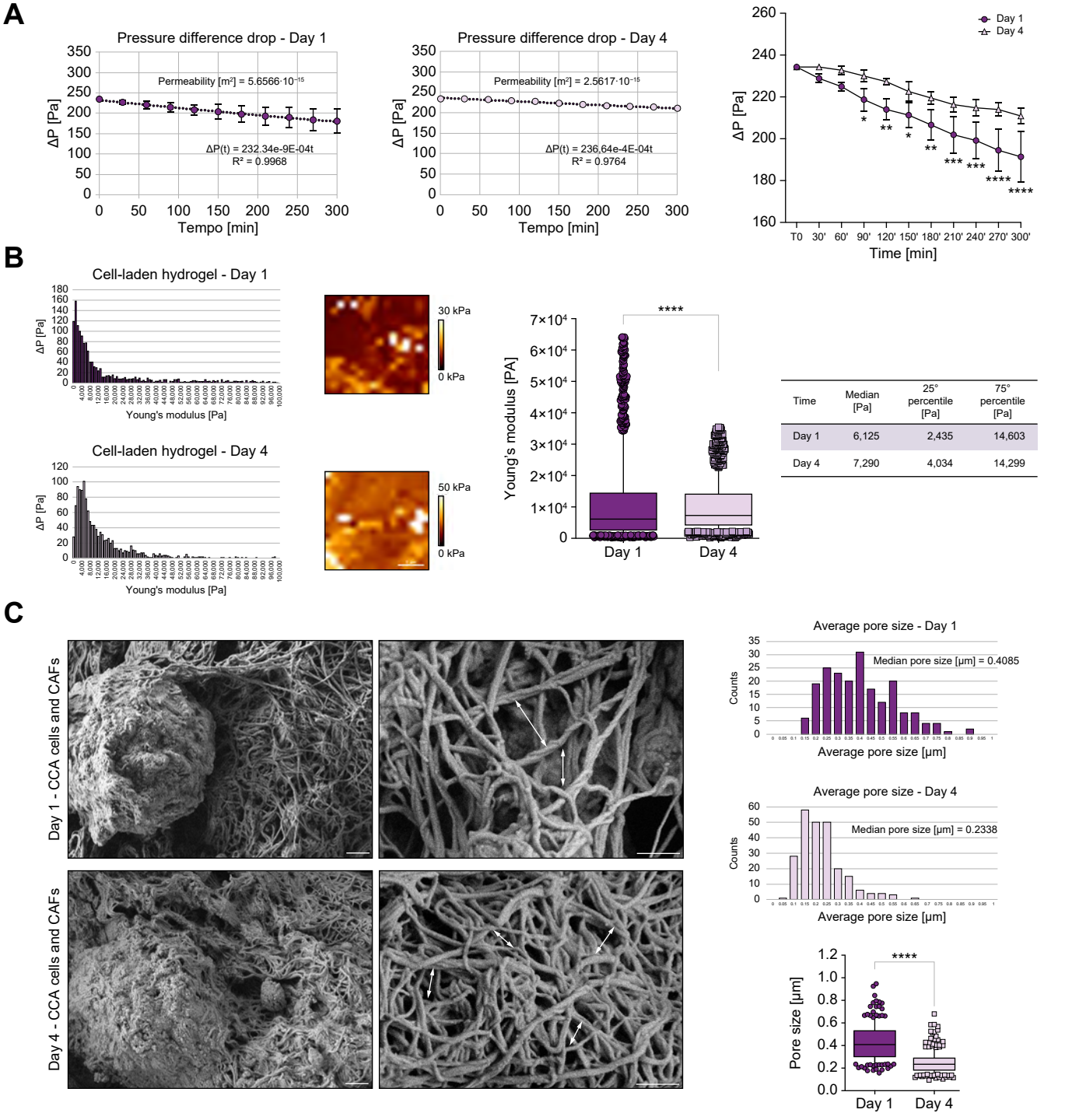

Fig. 2. Cell-laden hydrogel characterisation. (A) Pressure difference drop. Two-way ANOVA (mean ± SEM; n = 5 biological replicates). (B) Young's modulus distribution. Two representative Young's modulus force maps related to the local measurements. Mann-Whitney *U* test (median with IQR; n = five biological replicates). (C) Left, representative SEM images of the cell-laden hydrogel. Right, the hydrogel fibre images with the pore size distribution. Mann-Whitney *U* test (medians with interquartile range; n = 5 biological replicates). Scale bar = 1 μm *p <0.0001. CAFs, cancer-associated fibroblasts; CCA, cholangiocarcinoma.

unstimulated T cells were stained with CellTracker™ Green (Invitrogen) and injected in the chip endothelial channel at 15 × 10^6 cells/ml. To promote T cell adhesion to ECs in static conditions, 150 μl of medium were removed from the left lateral reservoirs, creating a hydrostatic pressure gradient, as reported in the literature.[15] Primary CCA cells and CAFs from 6 patients were used, divided into low-infiltrating (COLD; n = 3) and high-infiltrating patients (HOT; n = 3) according to the

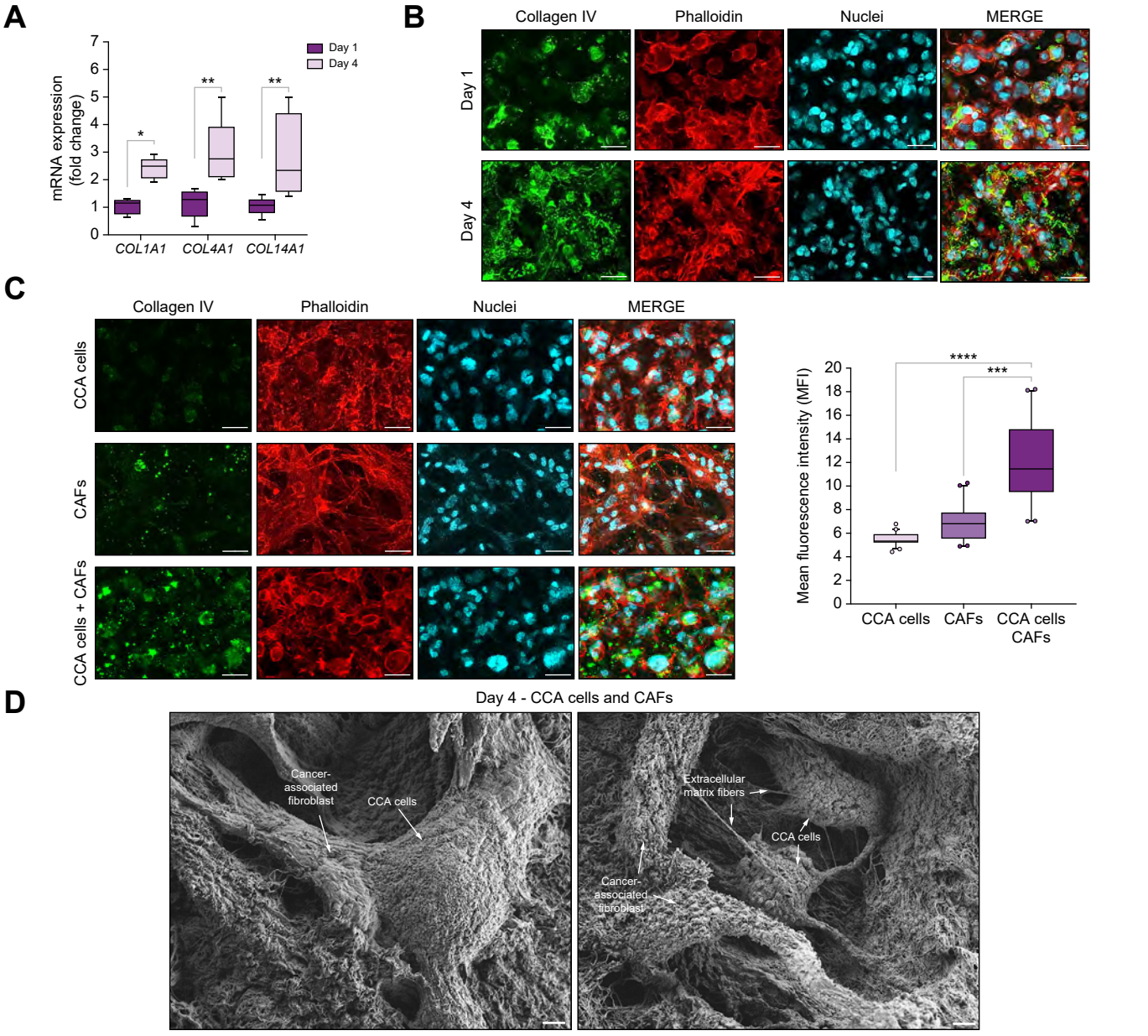

Fig. 3. Collagen deposition analysis on-chip. (A) Gene expression of extracellular matrix (ECM) proteins in the co-culture of CCA primary cells and CAFs. Two-way ANOVA (mean ± SEM; n = 5 biological replicates). (B) Representative confocal images for collagen IV (green), phalloidin (red), and nuclei (cyan) for CCA primary cells and CAFs co-culture. Scale bar = 50 μm. (C) Left, representative confocal images for collagen IV (green), phalloidin (red) and nuclei (cyan) on Day 4 for CCA primary cells and CAFs-on-chip. Scale bar = 50 μm. MFI of collagen IV staining. One-way ANOVA (medians with IQR; n = 5 biological replicates). (D) Representative SEM images of the device on Day 4. Scale bar = 2 μm *p <0.05; **p <0.01; ***p <0.0005; ****p <0.0001. CAFs, cancer-associated fibroblasts; CCA, cholangiocarcinoma; MFI, mean fluorescence intensity.

immunohistochemistry (IHC) analysis for CD3+ cells. The patient's characteristics are summarised in Tables S2, S3 and S4.

For further details regarding the materials and methods used, please refer to the CTAT table and supplementary information; including, MATLAB code used to calculate the dextran diffusion coefficient (Fig S3), Hydraulic permeability setup (Fig S4), Medium identification for cell co-culture on-chip (Fig S5), Hydrogel composition analysis and cell co-culture optimization (Fig S6), Dextran diffusion assay (Fig S7), and Bare Hydrogel Characterisations (Fig S8).

Results

The 3D model of CCA on a microfluidic device reproduces the architectural structure and maintains primary cells phenotype

A three-channel microfluidic device was designed to mimic the structure of this liver cancer and promote 3D cellular organisation and interactions. The CCA niche was recreated by co-culturing CCA cells and CAFs, flanked by ECs recreating a tubular structure. This design was prompted as a result of the well-recognised role of tumour cells and CAFs crosstalk in CCA.[6,7]

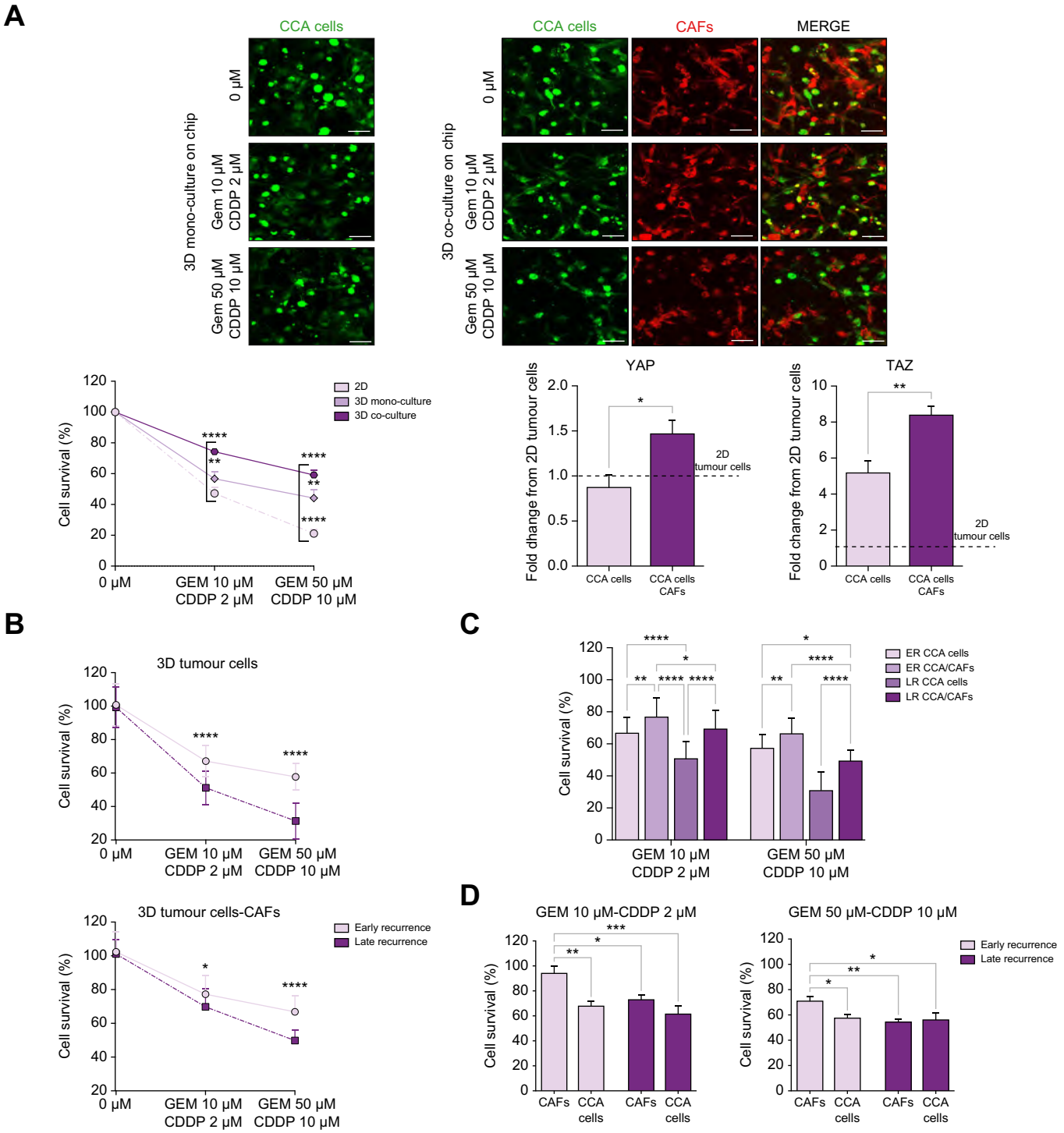

Fig. 4. GEM/CDPP exposure analysis. (A) At the top, representative confocal images of CCA cells in 3D mono-culture and in 3D co-culture on chip after drug treatment (48 h). Scale bar = 100 µm. At the bottom, dose–response curves for CCA primary cells (n = 5 patients) in 2D culture, 3D mono-culture and 3D co-culture. Two-way ANOVA (mean ± SEM; n = 5 biological replicates). Gene expression analysis for YAP and TAZ in 3D mono-culture and 3D co-culture. Mann-Whitney *U* test (mean ± SEM; n = 5 biological replicates). (B) Dose–response curves for 3D mono-culture and 3D co-culture on chip in early (ER; n = 3 patients) and late (LR; n = 2 patients) recurrence patients. Two-way ANOVA (mean ± SEM; n = 5 biological replicates). (C) Percentage of cell viability for the 3D mono-culture and the 3D co-culture in ER and LR patients. Two-way ANOVA (mean ± SEM; n = 5 biological replicates). (D) Percentage of cell viability in the 3D co-culture for CAFs and CCA cells singularly in ER and LR patients. Two-way ANOVA (mean ± SEM; n = 3 biological replicates). *p <0.05; **p <0.01; ***p <0.0005; ****p <0.0001. CAFs, cancer-associated fibroblasts; CCA, cholangiocarcinoma; CDDP, cisplatin; ER, early recurrence; GEM, gemcitabine; LR, late recurrence; TAZ, transcriptional coactivator with PDZ-binding motif; YAP, yes-associated protein.

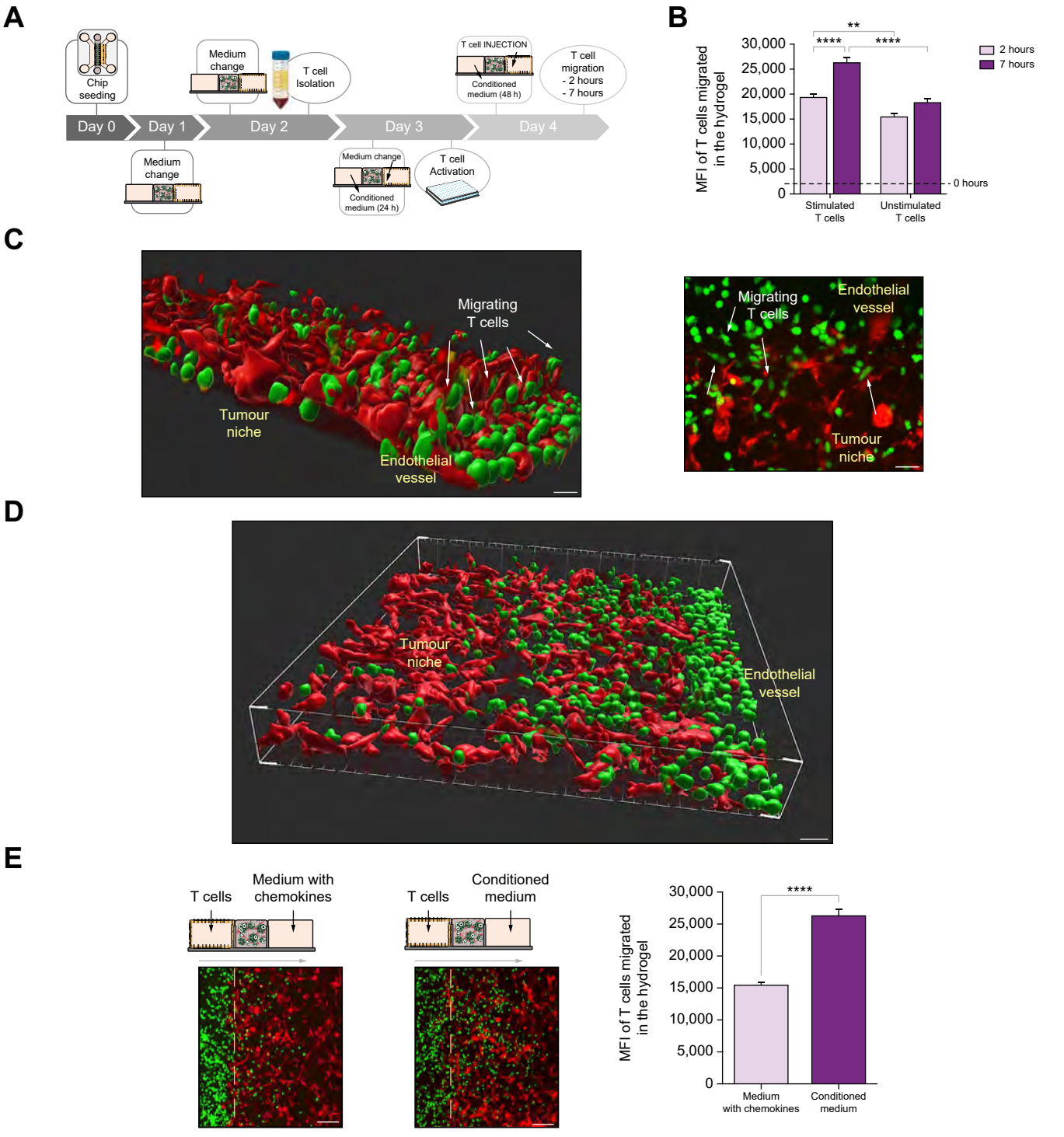

Fig. 5. Immune cells-on-chip. (A) Workflow of T cell migration assay on-chip. (B) MFI for stimulated and unstimulated T cells migrated in the hydrogel. Two-way ANOVA (mean ± SEM; n = 3 biological replicates). (C) Left, 3D surface rendering of z-stack using IMARIS. Scale bar = 15 μm. Right, representative confocal images of the migrating T cells in the tumour compartment. Scale bar = 20 μm. (D) 3D surface rendering of the device using IMARIS. Scale bar = 25 μm. (E) Left, representative confocal images of T cell migration with the medium supplemented with cytokines (CXCL9; CXCL10; CXCL11), compared with the chip-conditioned medium. Scale bar = 50 μm. Right, MFI of the green channel within the tumour compartment. Mann-Whitney *U* test (mean ± SEM; n = 5 biological replicates). T cells: green; CCA cells and CAFs: red. ****p <0.0001. CXCL9, C-X-C motif chemokine ligand 9; CXCL10, C-X-C motif chemokine ligand 10; CXCL11, C-X-C motif chemokine ligand 11; MFI, mean fluorescence intensity.

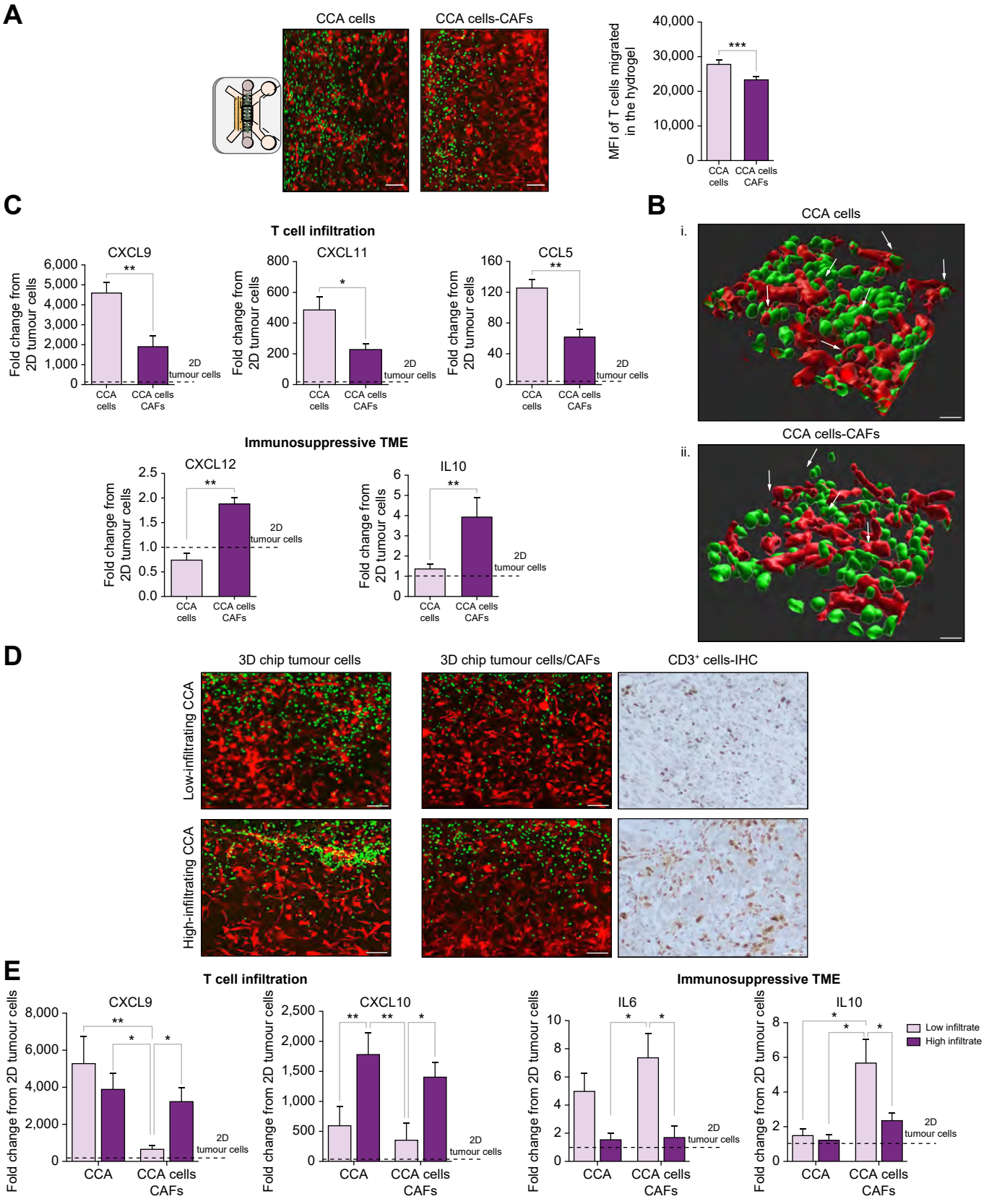

Fig. 6. T cell migration assay on-chip. (A) T cells migration through the tumour compartment (red) in 3D mono-culture of CCA cells alone and 3D co-culture of CCA cells and CAFs (n = 6 patients). Scale bar = 50 μm. Right, MFI of the green channel within the tumour compartment. Mann-Whitney *U* test (mean ± SEM; n = 5 biological replicates). (B) 3D surface rendering of the z-stack using IMARIS in the 3D mono-culture (i) and 3D co-culture (ii). T cells: green; CCA cells and CAFs: red. White arrows: interactions between T cells and CCA cells. Scale bar = 10 μm. (C) Gene expression analyses of T cell attractive and immunosuppressive

The three compartments were fluidically interconnected but separated by rows of pillars and featured independent inlet and outlet ports for individual injection of cells or medium. The central compartment was conceived to host the co-culture of CCA cells and CAFs with a width of 400 μm, intended as the distance between the minor bases of the trapezoidal pillars. The cell-laden hydrogel was injected into the central channel through the 1-mm diameter port. The optimised pillar distance (90 μm) ensured gel confinement, whereas their trapezoidal shape prevented bubble formation between the gel and the medium. The lateral channel is 1 mm wide, and the reservoir diameter is 8 mm, providing sufficient nutrient supply with one medium change per day. The right-side channel hosted ECs in a tubular structure (Fig. 1A). All three channels were 180 μm high.

Confocal microscopy analysis revealed the cellular spatial architecture on-chip. CCA cells organised into 3D spherical aggregates, surrounded by CAFs, showing an elongated bidimensional morphology (Fig. 1B). The ECs established a compact monolayer uniformly adhered to the side channel walls, recreating a complete tubular structure, emulating an endothelial vessel within the chip (Fig. 1C). Furthermore, the cells were able to well-retain their phenotype in this complex co-culture system, without undergoing dedifferentiation. On the 3D co-culture, cytokeratin (*CK*) 19 and epithelial cell adhesion molecule (*EpCAM*) expression significantly increased from Day 1 to Day 4 in CCA primary cells (Fig. 1D). Comparable results were observed when CCA cell lines (HuCCT1 and HuH28) were co-cultured with CAFs within the platform (Fig. S10E). In the 3D co-culture, a notable increase in the expression levels of alpha-smooth muscle actin (*αSMA*) and platelet-derived growth factor receptor beta (*PDGFRβ*) was observed even for CAFs (Fig. 1D). Moreover, CCA cells significantly enhanced the E-cadherin (*ECAD*) expression in a time-dependent manner within the device (Fig. 1D; Fig. S10E). Our results suggest that CCA cells begin to display a 3D morphology suddenly after 1 day in culture.[16,17]

The tumour niche undergoes a deep remodelling in the 3D device, with an increase in hydrogel stiffness and extracellular matrix deposition

To deeply characterise the tumour niche in the central channel, the changes in the mechanical and morphological matrix proprieties were assessed on Day 1 and Day 4. A significant reduction of the hydraulic permeability was observed (Fig. 2A), along with a noteworthy increase in the hydrogel stiffness on Day 4 compared with Day 1 (Fig. 2B). Interestingly, scanning electron microscopy analysis enabled precise evaluation of both the fibre morphology and hydrogel porosity, unveiling a considerable reduction in the median pore size of the hydrogel matrix on Day 4 (Fig. 2C). These results might reflect the established crosstalk between CCA cells and CAFs, eventually stimulating ECM protein deposition. Therefore, we evaluated the expression of collagen type I (*COL1A1*), IV (*COL4A1*) and XIV (*COL14A1*), overexpressed in CCA.[18,19] Over time in culture within the device, a notable upregulation in the expression of all collagen types analysed was observed (Fig. 3A). This upregulation was found to be correlated with a significant release of collagen IV in the chip microenvironment, surrounding the cell co-culture (Fig. 3B). The mean fluorescence intensity (MFI) of collagen IV increased by 30% (data not shown; p <0.0075) on Day 4. Interestingly, the collagen IV deposition was noticeable only in the 3D co-culture condition (Fig. 3C). Moreover, a significant upregulation in the expression of all three collagen types was observed in CCA cell lines (HuCCT1 and HuH28) when co-cultured within the device (Fig. S10F).

Our results highlighted that the hydrogel matrix microstructure undergoes important changes in our microfluidic device, leading to a consistent release of ECM proteins over time. These findings suggest that CCA cells and CAFs developed a deep and intricate interconnection with the matrix, which in turn sustains their growth and crosstalk (Fig. 3D).

Drug analysis on the CCA-on-chip: a reliable platform for drug exposure analysis and patient-specific drug testing

We evaluated the potential use of this microfluidic platform in drug-screening applications, using a combination of gemcitabine and cisplatin (GEM–CDDP),[20,21] on five CCA patient-derived cells. Tumour cells cultured in the 2D configuration showed a higher sensitivity to GEM–CDDP compared with the 3D monoculture (Fig. 4A), in agreement with known data.[22,23] Nevertheless, the response to GEM–CDPP treatment was significantly reduced when CCA cells were co-cultured with CAFs on-chip, compared with the 2D system and 3D monoculture (Fig. 4A). Among the mechanisms reported to potentially contribute to CCA drug resistance, the intracellular activation of the transcriptional co-activator yes-associated protein (YAP)/transcriptional co-activator with PDZ-binding motif (TAZ) pathway has been described.[24,25] In the 3D co-culture, a significant increase in *YAP* and *TAZ* expression was observed compared with both 2D and 3D monocultures (Fig. 4A).

Moreover, to assess the ability of the CCA-on-chip as a patient-specific platform, the drug response was evaluated by dividing CCA patients according to time to relapse after adjuvant therapy, namely as early (ER; <12 months) and late (LR; >12 months) recurrence groups. The patient's characteristics are summarised in Table S3. No statistically significant differences resulted among the two groups in terms of age, sex, tumour grading, staging, microvascular invasion, number and size of tumours, serum Ca-19.9, and the quality of the underlying liver.

The ER patients showed higher resistance to GEM–CDPP treatment compared with the LR patients, both in 3D monoculture and 3D co-culture with CAFs (Fig. 4B). Furthermore, the presence of CAFs in the cell culture conferred a greater resistance to drug exposure in both groups (Fig. 4C). Notably, analysing the viability of each cell population in the 3D co-culture, CCA cells and CAFs exhibited a comparable response to GEM–CDPP treatment in LR patients. However, in the ER patients, CAFs displayed significantly higher viability compared with CCA cells, suggesting that CAFs could play a role in the increased resistance observed with the GEM–CDPP treatment, with differences among the ER and LR patients (Fig. 4D).

These results corroborate that the 3D microenvironment, characterised by deep cell–cell and cell–ECM interactions, hampers the sensitivity to drug treatment, highlighting the

molecules. Mann–Whitney *U* test (mean ± SEM; n = 5 biological replicates). (D) Left, representative confocal images of low- (COLD; n = 3 patients) and high-infiltrating (HOT; n = 3 patients) CCA patients. Scale bar = 50 μm. Right, representative IHC images (CD3+ cells) of HOT and COLD patients. Scale bar = 100 μm. (E) Gene expression analyses of T cell attractive and immunosuppressive molecules in patients designated HOT and COLD. Two-way ANOVA (mean ± SEM; n = 5 biological replicates). *p <0.05; **p <0.01; ***p <0.0005; ****p <0.0001. CAFs, cancer-associated fibroblasts; CCA, cholangiocarcinoma; IHC, immunohistochemistry; MFI, mean fluorescence intensity; TME, tumour microenvironment.

relevance of this CCA-on-chip as a platform for patient-specific drug testing.

Integration of the immune cells on the CCA-on-chip results in a reliable 3D platform for interaction study of the tumour niche and immune system in CCA

T cells were integrated into the device to assess its reliability for immune-cell interaction studies. The workflow is resumed in Fig. 5A. Firstly, we examined the ability of stimulated T cells to migrate from the endothelial channel to the tumour niche compared with unstimulated T cells. A significantly higher migration was observed for stimulated T cells, increasing in a time-dependent manner (Fig. S9A; Fig 5B), confirming known data.[15,26]

The 3D reconstruction of the device allowed to appreciate the interactions between ECs and T cells during their extravasation into the tumour niche (Fig. 5C). The adhesion and elongation of T cells on the ECs provide further evidence of the functional integrity of the mimicked endothelial vessel. Moreover, despite the static condition of the device, T cells demonstrated the ability to migrate within the tumour niche, spreading throughout the central channel for its entire height (Fig. 5D).

Subsequently, the chemoattractant potential of the chip-conditioned medium (48 h) was assessed and compared to the medium supplemented with three C-X-C motif chemokine ligands (CXCL9, -10, -11), well-known for their pivotal role in T cell migration.[27] The presence of the chip-conditioned medium led to a significantly greater T cell trafficking, indicating that the biochemical environment of the device, comprising various cytokines, chemokines, and growth factors, could more accurately mimic the *in vivo* TME, thereby allowing T cell trafficking studies in a more reliable milieu (Fig. 5E).

T cell trafficking analysis on-chip

As our results showed that the crosstalk between tumour cells and CAFs is involved in the tumour niche remodelling and increased drug resistance, we investigated whether this crosstalk was also crucial for T cell migration in the TME.

In the 3D CCA monoculture, T cells exhibited higher spreading compared to the 3D co-culture with CAFs (Fig. 6A). The 3D reconstruction showed a different T cells arrangement: in the 3D monoculture, T cells organised themselves in aggregates within the tumour niche, surrounding tumour spheroids, whereas they appeared more dispersed in the 3D co-culture (Fig. 6B).

Furthermore, we evaluated the expression of several molecules involved in T cell recruitment or in driving the establishment of an immunosuppressive milieu (Fig. S9B; Fig. 6C), known to be released by tumour cells and CAFs.[28] Noteworthy, the immunosuppressive molecules were found to be higher in the 3D co-culture (Fig. 6C), suggesting that the crosstalk between tumour cells and CAFs has a key role in fostering an immunosuppressive microenvironment.

Besides, by stratifying CCA patient-derived cells into low-infiltrating (COLD, n = 3) and high-infiltrating (HOT, n = 3) according to IHC analysis for CD3+ cells (Fig. 6D), a higher T cell migration was observed in HOT patients. Furthermore, in patients who were designated as both HOT and COLD, T cells exhibited higher migration in the 3D monoculture compared to the 3D co-culture (Fig. S9C), suggesting the CAFs might have a role in modulating the levels of immune-cell chemoattractant molecules, as well as immunosuppressive ones (Fig. S9C). Notably, a significant decrease in the expression of *CXCL9* and *CXCL10* was observed in the 3D co-culture of COLD patients. Additionally, the expression of *IL6* was significantly lower in HOT patients in both culture conditions. Similar trends were observed for *IL10* expression (Fig. 6E). qRT-PCR data from different culture conditions and patients, indicate that CAFs are the primary source of *CXCL12* in the TME. Indeed, its expression is significantly higher in co-culture with CAFs compared with tumour cells alone. Furthermore, CAFs are the major source of IL10, as its expression increases sixfold in co-culture, whereas tumour cells release only a small amount of this molecule (Fig. 6C–E). These findings suggest that CXCL9 and CXCL10 could play a crucial role in the recruitment of immune cells in highly infiltrated patients. Conversely, IL6 and IL10 could potentially influence the immunosuppressive milieu in patients with low tumoral infiltrate.

Discussion

The past decade has seen significant advances in understanding the molecular pathogenesis of CCA, yet it remains a tumour with limited therapeutic options and high mortality. Although preclinical models of CCA are essential to accelerate the development of novel therapeutic strategies, current 2D and 3D *in vitro* models of CCA fail to recapitulate its highly desmoplastic TME, in which tumour cells and CAFs support each other in bidirectional crosstalk that promotes CCA proliferation, invasiveness, and drug resistance.[5,29] Further, none of the available *in vitro* models includes the immune infiltrate and, although CCA is mainly considered a cold tumour with little infiltrate, we and others have demonstrated the key role of the immune infiltrate in CCA pathogenesis.[30,31]

OoC technology is emerging as a powerful tool in cancer research, because of its ability to better mirror the complexity of the tumour niche compared with standard culture methods.

The tumour-on-chip recreates essential elements of an *in vivo* TME, such as cell–cell and cell–ECM interactions in a fine-controlled dynamic environment. This innovative system holds great promise as a valuable tool for high-throughput screening of anticancer drugs.[32,33] Despite the great success of microfluidic platforms for different types of cancers, few liver cancer-on-chip models have been established, but none aimed to recapitulate the CCA TME.[13,34]

The CCA-on-chip herein described aims to reconstruct the CCA niche with a co-culture of patient-derived tumour cells and CAFs, embedded in a stiff microenvironment that (i) provides cells with mechanical stimuli similar to those perceived in their *in vivo* milieu, (ii) allows their 3D spatial organisation, and (iii) promotes cell–cell interactions in a more physiological-like environment.

The tumour niche was flanked by an endothelial structure, conceived to simulate the intravenous administration of therapeutic molecules during drug testing. The device architectural reconstruction enabled the visualisation of the cell ability to self-organised into spherical aggregates surrounded by elongated CAFs. Moreover, the cells exhibited a better retaining of their key phenotypic markers within our model compared to 2D culture systems and 3D CCA monoculture. These findings suggest that our platform faithfully simulates the 3D topology of the *in vivo* CCA niche, thereby representing a powerful *in vitro* tumour model.

The biological functionality of the endothelial tubule was validated through diffusion analysis, enabling an accurate simulation of drug delivery. The device exhibited excellent biocompatibility, ensuring the free exchange of growth factors and signalling molecules across the three compartments, thereby fostering cell growth and cell–cell communication. Furthermore, the substantial deposition of ECM proteins pointed out the significant changes in matrix mechanical properties of the central channel, ascribed to the crosstalk established within the CCA-on-chip platform, thus functionally mimicking the extensive matrix remodelling observed in the *in vivo* TME.[19]

Drug exposure analysis revealed an increased drug resistance in the platform when patient-derived tumour cells were co-cultured with CAFs, compared with the conventional culture methods. Therefore, the intensive bidirectional crosstalk established between CCA cells, CAFs, and ECM proteins within our CCA-on-chip model could play a crucial role in the increased resistance to pharmacological treatments. Indeed, the stiffer hydrogel, attributable to ECM protein deposition, suggests that tumour niche-on-chip undergoes mechanical stresses similar to those in their *in vivo* milieu, which could activate the YAP/TAZ pathway and promote chemoresistance.

Notably, our model can recapitulate different drug responses based on patient characteristics (early recurrence *vs.* late recurrence groups).

Finally, T cells were integrated into the device to assess its reliability for immune cell interaction studies. The platform demonstrated higher T cell migration in patients with highly infiltrated tumours, confirming its ability to mimic the *in vivo* CCA niche and represent a reliable 3D platform for patient-specific immunological studies.

Notwithstanding these advantages and encouraging results, our study has some limitations. Firstly, our current system lacks a microfluidic pump, which could better mimic blood flow dynamics. The static condition for this CCA-on-chip was driven by the purpose to develop a device with a straightforward set-up, allowing experiments with multiple replicates. This approach was further achievable through the use of PDMS, a highly biocompatible material that allows an efficient oxygen exchange between the cells and the surrounding environment.[35] Secondly, although this CCA-on-chip demonstrated its ability to accurately recapitulate the *in vivo* CCA physiology, further clinical validation involving a larger patient cohort is required. Third, although the chip well integrates CAFs, CCA cells, and endothelial cells, the immune TME of the model is limited to T cells and excludes the innate immune system and other players of the adaptive immune system. Finally, despite the advantages of the CCA-on-chip, such as reduced biological material and reagent cost, its use currently required technological skill from the operator, hindering its systematic exploitation in clinical settings.

In conclusion, we herein present a reliable biomimetic *in vitro* model of CCA that accurately mirrors the *in vivo* CCA microenvironment. This model holds significant potential as a valuable tool for investigating patient-specific therapeutic strategies. Future advancements of the device might involve exploring the contributions of different subtypes of CAFs or T cells, sorted before their injection into the chip, to elucidate their crosstalk with tumour cells. These studies could provide insights into the heterogeneity of the CCA TME and the molecular mechanisms underlying its development, progression, and drug resistance. Moreover, based on the results obtained from drug treatments, further investigations can be conducted to unravel the pathways associated with different drug responses in patients with early and late disease recurrence.

Abbreviations

αSMA, alpha-smooth muscle actin; ACA, aminocaproic acid; CAFs, cancer-associated fibroblast; CCA, cholangiocarcinoma; CDDP, cisplatin; CK, cytokeratin; CXCL9, C-X-C motif chemokine ligand 9; CXCL10, C-X-C motif chemokine ligand 10; CXCL11, C-X-C motif chemokine ligand 11; ECM, extracellular matrix; ECs, endothelial cells; EPCAM, epithelial cell adhesion molecule; ER, early recurrence; GEM, gemcitabine; HEPES, 4-(2-hydroxyethyl)-1-piperazineethanesulfonic acid; IHC, immunohistochemistry; LoC, liver-on-chip; LR, late recurrence; MFI, mean fluorescence intensity; OoCs, organs-on-chip; PDGFRβ, platelet derived growth factor receptor beta; PDMS, polydimethylsiloxane; TAZ, transcriptional coactivator with PDZ-binding motif; TME, tumour microenvironment; YAP, yes-associated protein.

Financial support

The present work was funded by "Fondazione AIRC per la Ricerca sul Cancro" (IG2019 project number 23408 to AL).

Conflicts of interest

AL reports receiving consulting fees from Advanz Pharma, AlfaSigma, Takeda, and Albireo Pharma, and speaker fees from Gilead, AbbVie, MSD, Intercept Pharma, AlfaSigma, GSK, and Incyte. All other authors declare no conflicts of interest.

Please refer to the accompanying ICMJE disclosure forms for further details.

Authors' contributions

Study design and conceptualisation: MAP, SM, MR, AL. Sample collection and processing: MAP, CS, BF. Data acquisition, analysis, and interpretations: MAP, CS, EF, AR. Image analysis: MAP, CS, BF, GS, FDA. AFM analysis: MAP, AM, AR. Patient, clinical data, and liver specimen recruitment: GC, NP, MD, GT. Manuscript writing: MAP, MR, AL. Critical revision of the manuscript: SM, MR, AL, NP, MD, GT.

Data availability statement

The data that support the findings of this study are available from the corresponding author, upon reasonable request.

Acknowledgments

The device manufacture was partially performed at PoliFab, the micro- and nanofabrication facility of Politecnico di Milano, Milan, Italy.

Supplementary data

Supplementary data to this article can be found online at https://doi.org/10.1016/j.jhepr.2023.100910.

References

Author names in bold designate shared co-first authorship

[1] Banales JM, Marin JJG, Lamarca A, et al. Cholangiocarcinoma 2020: the next horizon in mechanisms and management. Nat Rev Gastroenterol Hepatol 2020;17:557–588.

[2] Izquierdo-Sanchez L, Lamarca A, La Casta A, et al. Cholangiocarcinoma landscape in Europe: diagnostic, prognostic and therapeutic insights from the ENSCCA Registry. J Hepatol 2022;76:1109–1121.

[3] Ilyas SI, Affo S, Goyal L, et al. Cholangiocarcinoma – novel biological insights and therapeutic strategies. Nat Rev Clin Oncol 2023;20:470–486.

[4] Turgeon MK, Maithel SK. Cholangiocarcinoma: a site-specific update on the current state of surgical management and multi-modality therapy. Chin Clin Oncol 2020;9:4.
[5] Calvisi DF, Boulter L, Vaquero J, et al. Criteria for preclinical models of cholangiocarcinoma: scientific and medical relevance. Nat Rev Gastroenterol Hepatol 2023;20:462–480.
[6] Affo S, Nair A, Brundu F, et al. Promotion of cholangiocarcinoma growth by diverse cancer-associated fibroblast subpopulations. Cancer Cell 2021;39:883.
[7] Filliol A, Saito Y, Nair A, et al. Opposing roles of hepatic stellate cell subpopulations in hepatocarcinogenesis. Nature 2022;610:356–365.
[8] Tsai H-F, Trubelja A, Shen AQ, et al. Tumour-on-a-chip: microfluidic models of tumour morphology, growth and microenvironment. J R Soc Interface 2017;14:20170137.
[9] Imamura Y, Mukohara T, Shimono Y, et al. Comparison of 2D- and 3D-culture models as drug-testing platforms in breast cancer. Oncol Rep 2015;33:1837–1843.
[10] Al Hrout A, Cervantes-Gracia K, Chahwan R, et al. Modelling liver cancer microenvironment using a novel 3D culture system. Sci Rep 2022;12:8003.
[11] **Wong BS**, **Shah SR**, Yankaskas CL, et al. A microfluidic cell-migration assay for the prediction of progression-free survival and recurrence time of patients with glioblastoma. Nat Biomed Eng 2021;5:26–40.
[12] van Riet S, van Schadewijk A, Khedoe PPSJ, et al. Organoid-based expansion of patient-derived primary alveolar type 2 cells for establishment of alveolus epithelial Lung-Chip cultures. Am J Physiol Lung Cell Mol Physiol 2022;322:L526–L538.
[13] Sun W, Chen Y-Q, Wang M-F, et al. Study on drug resistance to tumor cell in oxygen gradient and co-culture microfluidic chip. Chin J Anal Chem 2020;48:180–186.
[14] **Polidoro MA**, **Ferrari E**, Marzorati S, et al. Experimental liver models: from cell culture techniques to microfluidic organs-on-chip. Liver Int 2021;41:1744–1761.
[15] Mollica H, Teo YJ, Tan ASM, et al. A 3D pancreatic tumor model to study T cell infiltration. Biomater Sci 2021;9:7420–7431.
[16] Schmidt M, Scholz CJ, Polednik C, et al. Spheroid-based 3-dimensional culture models: gene expression and functionality in head and neck cancer. Oncol Rep 2016;35:2431–2440.
[17] Powan P, Luanpitpong S, He X, et al. Detachment-induced E-cadherin expression promotes 3D tumor spheroid formation but inhibits tumor formation and metastasis of lung cancer cells. Am J Physiol Cell Physiol 2017;313:C556–C566.
[18] Cadamuro M, Stecca T, Brivio S, et al. The deleterious interplay between tumor epithelia and stroma in cholangiocarcinoma. Biochim Biophys Acta Mol Basis Dis 2018;1864:1435–1443.
[19] Utispan K, Thuwajit P, Abiko Y, et al. Gene expression profiling of cholangiocarcinoma-derived fibroblast reveals alterations related to tumor progression and indicates periostin as a poor prognostic marker. Mol Cancer 2010;9:13.
[20] **Kim BJ**, **Hyung J**, Yoo C, et al. Prognostic factors in patients with advanced biliary tract cancer treated with first-line gemcitabine plus cisplatin: retrospective analysis of 740 patients. Cancer Chemother Pharmacol 2017;80:209–215.
[21] Shroff RT, Javle MM, Xiao L, et al. Gemcitabine, cisplatin, and nab-paclitaxel for the treatment of advanced biliary tract cancers: a phase 2 clinical trial. JAMA Oncol 2019;5:824–830.
[22] **Melissaridou S**, **Wiechec E**, Magan M, et al. The effect of 2D and 3D cell cultures on treatment response, EMT profile and stem cell features in head and neck cancer. Cancer Cell Int 2019;19:16.
[23] Muguruma M, Teraoka S, Miyahara K, et al. Differences in drug sensitivity between two-dimensional and three-dimensional culture systems in triple-negative breast cancer cell lines. Biochem Biophys Res Commun 2020;533:268–274.
[24] **Pei T**, **Li Y**, **Wang J**, et al. YAP is a critical oncogene in human cholangiocarcinoma. Oncotarget 2015;6:17206–17220.
[25] Cigliano A, Zhang S, Ribback S, et al. The Hippo pathway effector TAZ induces intrahepatic cholangiocarcinoma in mice and is ubiquitously activated in the human disease. J Exp Clin Cancer Res 2022;41:192.
[26] de Haan L, Suijker J, van Roey R, et al. A microfluidic 3D endothelium-on-a-chip model to study transendothelial migration of T cells in health and disease. Int J Mol Sci 2021:22.
[27] Tokunaga R, Zhang W, Naseem M, et al. CXCL9, CXCL10, CXCL11/CXCR3 axis for immune activation – a target for novel cancer therapy. Cancer Treat Rev 2018;63:40–47.
[28] **Caligiuri A**, **Pastore M**, Lori G, et al. Role of chemokines in the biology of cholangiocarcinoma. Cancers (Basel) 2020;12:2215.
[29] Brivio S, Cadamuro M, Strazzabosco M, et al. Tumor reactive stroma in cholangiocarcinoma: the fuel behind cancer aggressiveness. World J Hepatol 2017;9:455–468.
[30] **Alvisi G**, **Termanini A**, Soldani C, et al. Multimodal single-cell profiling of intrahepatic cholangiocarcinoma defines hyperactivated Tregs as a potential therapeutic target. J Hepatol 2022;77:1359–1372.
[31] Greten TF, Schwabe R, Bardeesy N, et al. Immunology and immunotherapy of cholangiocarcinoma. Nat Rev Gastroenterol Hepatol 2023;20:349–365.
[32] Lanz HL, Saleh A, Kramer B, et al. Therapy response testing of breast cancer in a 3D high-throughput perfused microfluidic platform. BMC Cancer 2017;17:709.
[33] Hassell BA, Goyal G, Lee E, et al. Human organ chip models recapitulate orthotopic lung cancer growth, therapeutic responses, and tumor dormancy in vitro. Cell Rep 2017;21:508–516.
[34] Lu S, Cuzzucoli F, Jiang J, et al. Development of a biomimetic liver tumor-on-a-chip model based on decellularized liver matrix for toxicity testing. Lab Chip 2018;18:3379–3392.
[35] Rao H-X, Liu F-N, Zhang Z-Y. Preparation and oxygen/nitrogen permeability of PDMS crosslinked membrane and PDMS/tetraethoxysilicone hybrid membrane. J Memb Sci 2007;303:132–139.